Journal of
Materials Chemistry C

PAPER

View Article Online
View Journal | View Issue

Cite this: J. Mater. Chem. C, 2015, 3, 4407

Exploiting single-molecule magnets of β-diketone dysprosium complexes with C_{3v} symmetry: suppression of quantum tunneling of magnetization†

Yanping Dong,[ab] Pengfei Yan,[a] Xiaoyan Zou,[a] Tianqi Liu[a] and Guangming Li*[a]

Received 1st February 2015, Accepted 23rd March 2015

DOI: 10.1039/c5tc00321k

www.rsc.org/MaterialsC

A series of four β-diketone mononuclear dysprosium complexes, namely, $Dy(EIFD)_3(H_2O)\cdot CH_2Cl_2$ (**1**), $Dy(EIFD)_3(DMF)\cdot CH_2Cl_2$ (**2**), $Dy(EIFD)_3(DMSO)$ (**3**), and $Dy(EIFD)_3(TPPO)$ (**4**) (EIFD: 1-(1-ethyl-1*H*-indol-3-yl)-4,4,4-trifluorobutane-1,3-dione, TPPO: triphenylphosphine oxide), have been isolated by the reactions of a newly designed β-diketone EIFD, $DyCl_3\cdot 6H_2O$ and DMF, DMSO, TPPO, respectively. X-ray crystallographic analysis reveals that complexes **1–4** are isomorphic mononuclear structures in which the Dy(III) ion is rarely seven-coordinated with C_{3v} geometry. Magnetic studies indicate that all complexes **1–4** are single-molecule magnets. The correlations between magnetism and the distortion of the coordination symmetry around the Dy(III) ions have been investigated. Notably, the quantum tunneling of magnetization (QTM), which universally exists in the lanthanide complexes, has been effectively suppressed in this system more related to the less deviation from the ideal C_{3v} symmetry.

Introduction

The spins of single metal centers potentially acting as magnets are coupled with large intrinsic magnetic anisotropy.[1] Molecules exhibiting such behavior are called Single-Molecule Magnets (SMMs) or Single-Ion Magnets (SIMs).[2] Since the discovery that $Mn_{12}OAc$[3] exhibits SMM features, it has received considerable attention in the past two decades owing to its quantum tunneling and slow relaxation of molecular origin.[4] This has led to the opportunity of potential applications in memory storage, quantum computing, molecular spintronics and other devices.[5] An area of particular concern is improving the knowledge of the magneto-chemical properties of SMMs, leading to the persistent investigation of 4f lanthanide elements as magnetic centers,[6] which may bring significant anisotropy to the system. Then, the Ln(III) ion of particular interest is usually the Dy(III) ion due to its large magnetic moment and odd-electron configuration.[7] As a result, a large number of Dy-based SMMs or SIMs of mononuclear, multinuclear and chain forms have been reported.[2c,8] In particular, the mononuclear Dy(III) ion complexes have been at the forefront of major advances in the field of SMMs yielding higher effective energy barriers for spin reversal and higher blocking temperatures.[9] While the energy barriers change through alternation of coordination geometry around the center Dy(III) ion.[10] Obviously, the geometry of the ligand field (LF) is the most important factor to construct the magnetic anisotropy of SMMs or SIMs since the dynamic magnetism is governed by the ground-multiplet substructure.[2d,11] Theoretical and experimental studies have demonstrated that LF can split the $(2J + 1)$-fold ground state of the Ln(III) ion, which can stabilize sublevels with a large $|M_J|$ value.[12] It is interesting that the spin dynamics can be modified by the careful adjustment of the ligand around the Ln(III) ion center, achieving an easy axis of magnetization.[13] Thus it is significant to study how to obtain the magnetism of Dy(III) ion based SMMS or SIMs *via* a suitable ligand field. However, despite many mononuclear Dy(III) ion complexes having been studied, there is a lack of a complete and comparative theory on understanding the relationship between the structure and magnetism.

Notably, β-diketone ligands, which are important in sensitizing the luminescence of lanthanide complexes,[14] have generated increasing interest in the field of SMMs[15] because of a high-order single axis defining the local symmetry and providing a suitable ligand field.[7,13,16] So far, eight-coordinated β-diketone dysprosium complexes[2d,10,17] with D_{4d} or D_{2d} symmetry and nine-coordinated[7] β-diketone dysprosium complexes are familiar to chemistry

---

[a] Key Laboratory of Functional Inorganic Material Chemistry (MOE), School of Chemistry and Materials Science, Heilongjiang University, No. 74, Xuefu Road, Nangang District, Harbin, Heilongjiang 150080, P. R. China. E-mail: gmli_2000@163.com; Fax: +86-451-86608458, +86-451-86673647; Tel: +86-451-86608458

[b] Department of Food and Pharmaceutical Engineering, Suihua University, Suihua, Heilongjiang 152061, P. R. China

† Electronic supplementary information (ESI) available: FT-IR spectra, UV spectra, additional magnetic measurements, powder X-ray diffraction, selected bond lengths and angles for complexes **1–4**. CCDC 1039484–1039487. For ESI and crystallographic data in CIF or other electronic format see DOI: 10.1039/c5tc00321k

researchers, and all show the fast zero-field quantum tunneling of magnetization (QTM). Nevertheless, low-coordinated β-diketone dysprosium complexes, *e.g.* seven-coordinated complexes, have never been reported. Furthermore, lowering the coordination number can efficiently suppress the zero-field QTM, which drives Dy(III) ion complexes to behave as strong SMMs.[1a] Keeping it in mind, a series of mononuclear seven-coordinated β-diketone dysprosium complexes with a local symmetry close to a C_{3v}-capped octahedron have been originally synthesized by using a newly designed β-diketone, namely, 1-(1-ethyl-1*H*-indol-3-yl)-4,4,4-trifluorobutane-1,3-dione. Magnetic analysis reveals that all complexes **1–4** are single-molecule magnets. Herein, the correlation between the coordination geometry of the Dy(III) ion and the magnetism of the complexes has been discussed, quantified by some parameters of judging the symmetry of the ligand field.

Experimental section

Materials and instruments

Dysprosium oxide (Dy_2O_3, 99.99%) was purchased from Gan Zhou rare earth Chemical Plant (Jiang Xi, China). Triphenylphosphine oxide (98%, A. R.) was purchased from Beijing Fine Chemical Co. (Beijing, China), and 1-(1*H*-indol-3-yl) ethanone and ethyl trifluoroacetate were purchased from Shanghai D&R Finechem Co. (Shanghai, China). All chemicals except $DyCl_3{\cdot}6H_2O$ and EIFD were obtained from commercial sources and used without further purification. $DyCl_3{\cdot}6H_2O$ was prepared by the reactions of Dy_2O_3 and HCl in aqueous solution. Elemental (C, H and N) analyses were performed on a Perkin-Elmer 2400 analyzer. FT-IR spectra were collected on a Perkin-Elmer 100 spectrophotometer by using KBr pellets in the range of 4000–450 cm^{-1}. UV spectra were recorded on a Perkin-Elmer Lambda 35 spectrometer. Powder X-ray diffraction (PXRD) data were recorded on a Rigaku D/Max-3B X-ray diffractometer with CuKα as the radiation source (λ = 0.15406 nm) in the angular range of θ = 5–50° at room temperature. The magnetic susceptibilities of complexes **1–4** were measured using a Quantum Design VSM superconducting quantum interference device (SQUID) magnetometer. The magnetic corrections were obtained by using Pascal's constants.

Synthesis of 1-(1-ethyl-1*H*-indol-3-yl)ethanone (EIE)

1-(1*H*-Indol-3-yl)ethanone (1.5920 g, 10.0 mmol), NaOH (0.4000 g, 10.0 mmol) and C_2H_5Br (1.3248 g, 12.2 mmol) were added into acetone (150 mL), and the mixed solution was heated to reflux until the reaction was over. The product was isolated by solvent evaporation and acidified to pH 2–3 using hydrochloric acid (2 M solution). Then, the suspension was extracted twice with CH_2Cl_2 (30 mL). The organic layer was dried over Na_2SO_4, and the solvent was evaporated leading to a buff solid. The procedure can be seen as shown in Scheme S1 (ESI†). (1.5895 g, yield of 85% based on 1-(1*H*-indol-3-yl)ethanone). Elemental analysis (%) calcd for $C_{12}H_{13}NO$ (187.24): C, 76.97; H, 6.94. Found: C, 76.95; H, 6.97. ^1H NMR (400 MHz, $CDCl_3$) δ 15.86 (s, 1H), 8.24 (d, *J* = 4.4 Hz, 1H), 7.91 (s, 1H), 7.15-7.55 (m, 3H), 6.37 (s, 1H), 4.26 (dd, *J* = 14.0, 6.9 Hz, 2H), 1.57 (t, *J* = 7.0 Hz, 3H). *m*/*z* = 187.1 (M^+).

Synthesis of 1-(1-ethyl-1*H*-indol-3-yl)-4,4,4-trifluorobutane-1,3-dione (EIFD)

A typical procedure of Claisen Condensation was used, as shown in Scheme S2, ESI.† EIE (1.4979 g, 8.0 mmol) and ethyl trifluoroacetate (1.2785 g, 9.0 mmol) were added into toluene (30 mL), and the mixed solution was allowed to stir for 10 min. To this solution, *t*-BuOK (1.0099 g, 9.0 mmol) was added into the mixture till the reaction was over. The resulting solution was quenched with water and acidified to pH 2–3 using hydrochloric acid (2 M solution). Then, the suspension was extracted twice with CH_2Cl_2 (50 mL). The organic layer was dried over Na_2SO_4, and the solvent was evaporated leading to a buff solid. The buff solid product was isolated by recrystallization from ethanol (1.6995 g, yield of 75% based on EIE). Elemental analysis (%) calcd for $C_{14}H_{12}F_3NO_2$ (283.25): C, 59.36; H, 4.24. Found: C, 59.37; H, 4.27. IR (KBr, ν/cm^{-1}): 3433 (s), 1530 (s), 1277 (s), 1212 (s), 1144 (s), 750 (m). ^1H NMR (400 MHz, $CDCl_3$): δ 15.86 (s, 1H), 8.24 (d, *J* = 4.4 Hz, 1H), 7.91 (s, 1H), 7.15–7.55 (m, 3H), 6.37 (s, 1H), 4.26 (dd, *J* = 14.0, 6.9 Hz, 2H), 1.57 (t, *J* = 7.0 Hz, 3H). *m*/*z* = 283.08 (M^+).

Synthesis of $Dy(EIFD)_3(H_2O){\cdot}CH_2Cl_2$ (1)

Complex **1** was prepared by mixing EIFD (0.4249 g, 1.5 mmol), NaOH (0.0600 g, 1.5 mmol) and $DyCl_3{\cdot}6H_2O$ (0.1885 g, 0.5 mmol) in CH_3OH for 24 h at room temperature. Single crystals suitable for XRD were obtained from dichloromethane/hexane in 5 or 7 days. Yield: 1.4154 g (85.0%). Elemental analysis (%) calcd for $C_{43}H_{35}DyF_9N_3O_7$ (1110.14): C, 46.52; H, 3.15; N, 3.79. Found: C, 46.50; H, 3.18; N, 3.83. IR (KBr, ν/cm^{-1}): 3378 (s), 1589 (s), 1539 (s), 1383 (s), 1281 (s), 1214 (s), 1127 (s), 799 (w), 669 (m). UV-Vis (CH_3OH, λ_{max}/nm): 218, 265 and 386.

Synthesis of $Dy(EIFD)_3(DMF){\cdot}CH_2Cl_2$ (2)

Complex **2** was prepared by mixing complex **1** (0.0555 g, 0.05 mmol) and an appropriate amount of DMF. Single crystals suitable for XRD were obtained from dichloromethane/hexane in 2 or 3 days. Yield: 0.0988 g (88.0%). Elemental analysis (%) calcd for $C_{91}H_{78}Cl_2Dy_2F_{18}N_8O_{14}$ (2245.52): C, 48.67; H, 3.47; N, 4.99. Found: C, 48.60; H, 3.51; N, 4.95. IR (KBr, ν cm^{-1}): 2990 (w), 1600 (s), 1543 (s), 1375 (s), 1281(s), 1215 (s), 1129 (s), 791 (s), 744 (m), 668 (m). UV-Vis (CH_3OH, λ_{max}/nm): 213, 267 and 354.

Synthesis of $Dy(EIFD)_3(DMSO)$ (3)

Complex **3** was prepared by mixing complex **1** (0.0555 g, 0.05 mmol) and an appropriate amount of DMSO. Single crystals suitable for XRD were obtained from dichloromethane/hexane in 2 or 3 days. Yield: 0.0473 g (87.0%). Elemental analysis (%) calcd for $C_{44}H_{39}DyF_9N_3\ O_7S$ (1087.35): C, 48.60; H, 3.59; N, 3.87. Found: C, 48.66; H, 3.62; N, 3.84. IR (KBr, ν/cm^{-1}): 2990 (w), 1599 (s), 1543 (s), 1375 (s), 1279 (s), 1214 (s), 1129 (s), 801 (s), 744 (m), 669 (m). UV-Vis (CH_3OH, λ_{max}/nm): 214, 267 and 354.

Synthesis of $Dy(EIFD)_3(TPPO)$ (4)

Complex **4** was prepared by mixing equimolar quantities of complex **1** (1.1110 g, 1.0 mmol) and triphenylphosphine oxide

Table 1 Crystal data and structure refinement for complexes **1–4**

Complexes	**1**	**2**	**3**	**4**
Empirical formula	$C_{43}H_{35}Cl_2DyF_9N_3O_7$	$C_{91}H_{78}Cl_2Dy_2F_{18}N_8O_{14}$	$C_{44}H_{39}DyF_9N_3O_7S$	$C_{60}H_{48}DyF_9N_3O_7P$
Formula weight	1110.14	2245.52	1087.35	1287.49
Color	Buff	Buff	Buff	Buff
Crystal system	Triclinic	Triclinic	Triclinic	Triclinic
Space group	$P\bar{1}$	$P\bar{1}$	$P\bar{1}$	$P\bar{1}$
a (Å)	12.8051(4)	12.928(5)	12.2553(6)	12.960(5)
b (Å)	13.0203(4)	13.333(5)	13.2445(6)	13.524(5)
c (Å)	15.2674(6)	15.388(5)	15.0997(7)	18.921(5)
α (deg)	101.396(3)	94.383(5)	94.560(4)	70.340(5)
β (deg)	102.641(3)	100.445(5)	93.878(4)	81.202(5)
γ (deg)	109.004(3)	109.447(5)	109.954(4)	62.275(5)
V (Å^3)	2246.47(13)	2432.7(15)	2284.71(19)	2764.4(17)
Z	2	1	2	2
ρ (g cm^3)	1.641	1.533	1.581	1.547
μ (mm^{-1})	1.872	1.677	1.769	1.467
$F(000)$	1102.0	1120.0	1086.0	1294.0
R_1,[a] $[I > 2\sigma(I)]$	0.0391	0.0563	0.0352	0.0373
wR_2,[b] $[I > 2\sigma(I)]$	0.0837	0.1552	0.0907	0.0932
R_1,[a] (all data)	0.0526	0.0666	0.0414	0.0436
wR_2,[b] (all date)	0.0874	0.1646	0.0958	0.0987
GOF on F^2	0.980	1.040	1.018	1.039

[a] $R_1 = \sum||F_o| - |F_c||/|F_0|$. [b] $wR_2 = [\sum w(F_o{}^2 - F_c{}^2)^2/\sum w(F_o{}^2)^2]^{1/2}$.

(0.2783 g, 1.0 mmol) in CH_3OH for 24 h at room temperature. Single crystals suitable for XRD were obtained from dichloromethane/hexane in 5 or 7 days. Yield: 1.0944 g (85.0%). Elemental analysis (%) calcd for $C_{60}H_{48}DyF_9N_3O_7P$ (1287.49): C, 55.97; H, 3.73; N, 3.26. Found: C, 55.94; H, 3.77; N, 3.29. IR (KBr, ν cm^{-1}): 2982 (w), 1599 (s), 1537 (s), 1379 (s), 1279 (s), 1179 (s), 1129 (s), 794 (m), 748 (m), 668 (m), 541 (s). UV-Vis (CH_3OH, λ_{max}/nm): 213, 266 and 357.

X-ray crystallography

Single-crystal X-ray data of complexes **1–4** were collected on an Oxford Xcalibur Gemini Ultra diffractometer with graphite-monochromated Mo Kα (λ = 0.71073 Å) at room temperature. Empirical absorption corrections based on equivalent reflections were applied. The structures of complexes **1–4** were solved by direct methods and refined by full-matrix least-squares methods on F^2 using a SHELXS-97 crystallographic software package.[18] All non-hydrogen atoms are anisotropically refined. All crystal data and structure refinement details for complexes **1–4** are summarized in Table 1. The selected bond lengths and angles for complexes **1–4** are given in Table S1 (ESI†).

Results and discussion

Synthesis and spectral analysis of complexes 1–4

Ligands and complexes **1–4** were synthesized as shown in Schemes S1–S3, ESI.† The IR spectrum of complex **1** exhibits the typical broad absorption in the region 3000–3500 cm^{-1}, which proposes the presence of water molecules in the complex **1** (Fig. S1, ESI†). In contrast, the absence of a broad band in the region 3000–3500 cm^{-1} for complexes **2**, **3** and **4** suggests that the water molecules have been substituted by the neutral donors.[19] The UV-Vis spectra show that there are obvious absorption bands at around 384 nm for EIFD and 357 nm for complexes **1–4** (Fig. S2, ESI†), which result from the singlet–singlet π–π* enol absorption of the β-diketonate. In comparison with the absorption band of EIFD, the absorption maxima are blue-shifted 27 nm for complexes **1–4**, which result from the perturbation of the coordination of the Dy(III) ion.

PXRD analysis of complexes 1–4

Powder X-ray diffraction (PXRD) patterns of complexes **1–4** are in agreement with the simulated patterns (Fig. S12–15, ESI†). PXRD analysis further demonstrates that the crystal structures of complexes **1–4** are truly representative of the bulk materials. The differences in intensity are due to the preferred orientation of the powder samples.

Structural descriptions of 1–4

X-ray crystallographic analysis reveals that complexes **1–4** are all mononuclear structures and they crystallize in the triclinic space groups $P\bar{1}$. The central Dy(III) ions in complexes are all seven-coordinated to six oxygen atoms from three EIFD ligands and one oxygen atom from H_2O, DMF, DMSO and TPPO molecules (Fig. 1a–d). The average bond length of the Dy–O (EIFD oxygen atoms) is 2.302 Å for **1**, which is slightly shorter than that of Dy–O (water oxygen atom, 2.379 Å). This is attributed to the stronger ionic bond of Dy–O (EIFD oxygen atoms) compared to the covalent bond of Dy–O (water oxygen atoms). In the structures of complexes **2–4** (Fig. 1b–d), one H_2O molecule is substituted by another oxygen atom from DMF, DMSO, and TPPO, respectively. The average bond length of the Dy–O is 2.309 Å, 2.309 Å, and 2.311 Å for complexes **2–4**. It is notable that the intermolecular forces in complexes **2** and **3** are similar but different from complex **4**.

Obviously, the coordination geometries of the Dy(III) ion in complexes **1–4** are all distorted C_{3v}-capped octahedrons (Fig. 1e–h) according to the semiquantitative method of polytopal analysis.[20]

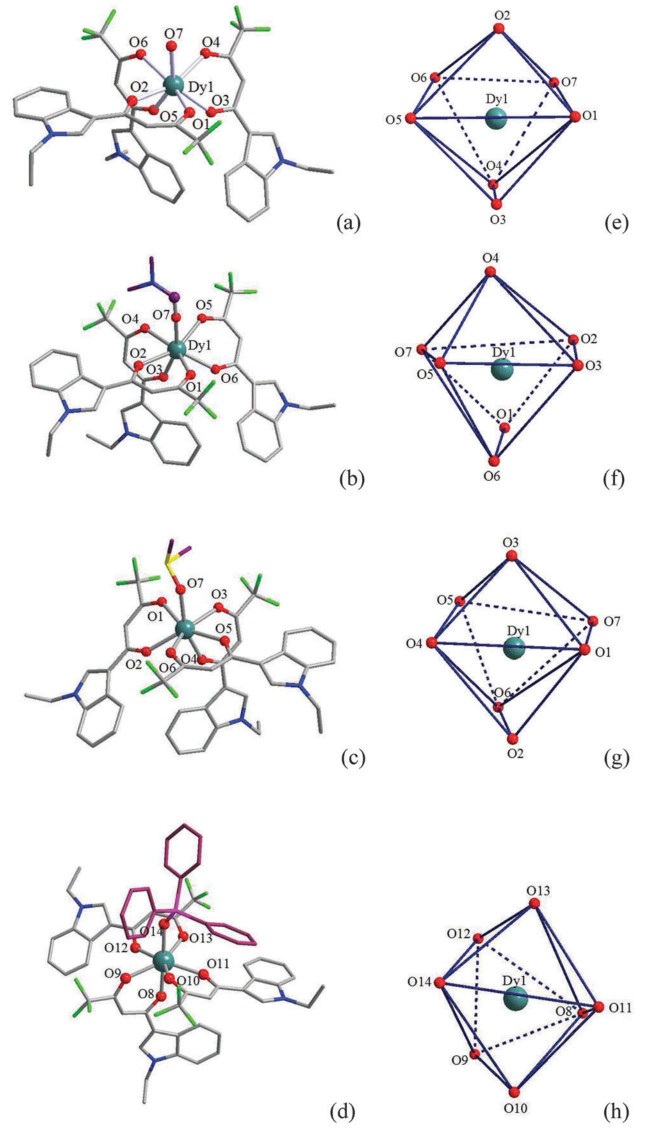

Fig. 1 The crystal structures of complexes **1** (a), **2** (b), **3** (c) and **4** (d) showing general ligand configurations. Local coordination geometry of the Dy(III) ion for complexes **1** (e), **2** (f), **3** (g) and **4** (h) (hydrogen atoms are omitted for clarity).

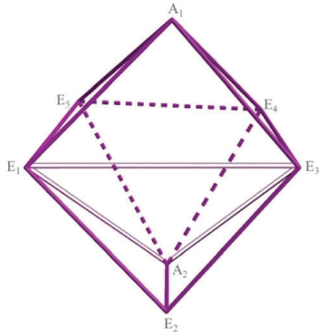

Fig. 2 C_{3v}-capped octahedron shape characteristics. The δ angles listed are associated with edges identified by double lines.

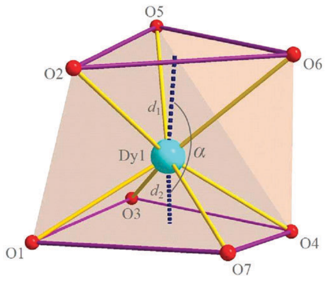

Fig. 3 Coordination geometry of Dy(III) core with d_1 and d_2 representing the distance of Dy(III) ion to the centers of the top plane and bottom plane and the bending angle α, defined as the angle of center-Dy(III)-center.

Relevant dihedral δ angles for complexes **1–4** are summarized in Table 2. The δ angles are descripted in Fig. 2. The angle data for the ideal and observed ML_7 structures are all 24.2° for the three δ values. We notice first of all that, for the complex **1**, δ_1, δ_2 and δ_3 are 11.8, 23.2 and 13.1°, which are close to an ideal C_{3v}-capped octahedron. δ_1 and δ_3 values are almost equal indicating a higher symmetry coordination sphere. For complexes **2–4**, the δ values deviate more from an ideal C_{3v}-capped octahedron in which complexes **2** and **3** are similar, having a lower coordination symmetry than that for complex **1**. However, complex **4** is midway between the C_{3v}-capped octahedron and C_{2v} monocapped trigonal prism, indicating the most distorted and lowest symmetry among the four complexes.

Moreover, another kind of representation of coordination geometries is also discussed, including l, d and α (Fig. 3). Detailed structural parameters of the Dy(III) ion such as plane center distances (d_1 and d_2), the plane center distance (l), and bending angles of center-Dy(III)-center (α) for complexes **1–4** are summarized in Table 3. It is noted that the distances from the centre of the Dy(III) ion to the two planes are different from complexes **1–4**. The distances in complex **1** are the shortest, those in complex **4** are the longest and those in complexes **2–3** are in the middle.

Magnetic properties

Static magnetic properties

In order to probe the magnetic behavior of complexes **1–4**, direct current (dc) magnetic susceptibility studies of **1–4** have

Table 2 δ (deg) values for complexes **1–4**

Faces	1		2		3		4		C_{3v}
δ_1	$O_2[O_1O_5]O_3$	11.8	$O_6[O_5O_3]O_4$	23.8	$O_3[O_1O_4]O_2$	28.5	$O_{13}[O_{11}O_{14}]O_{10}$	32.7	24.2
δ_2	$O_3[O_4O_5]O_6$	23.2	$O_7[O_1O_5]O_6$	3.6	$O_5[O_4O_6]O_2$	25.2	$O_{10}[O_9O_{14}]O_{12}$	42.2	24.2
δ_3	$O_3[O_1O_4]O_7$	13.1	$O_2[O_1O_3]O_6$	22.7	$O_7[O_1O_6]O_2$	13.9	$O_{11}[O_8O_{10}]O_9$	32.5	24.2

Table 3 Summary of Dy to plane center distances, plane center distances and bending angles for complexes **1–4**[21]

	1	**2**	**3**	**4**
Dy to top plane center distance (d_1, Å)	1.5647	1.5891	1.5926	1.6053
Dy to bottom plane center distance (d_2, Å)	1.0768	1.1015	1.0856	1.1095
Center distance between top and bottom planes (l, Å)	2.6368	2.6904	2.6561	2.7134
Bending angle (α, deg)	173.072	178.579	175.278	176.313

been carried out in an applied magnetic field of 100 Oe over the temperature range 300–1.8 K.[22] As shown in Fig. 4, the observed $\chi_m T$ products at 300 K are 14.11, 14.02, 14.10, and 14.09 cm^3 K mol^{-1} for **1**, **2**, **3** and **4**, respectively, in agreement with the $g = 4/3$ of the $^6H_{15/2}$ ground state of the Dy(III) ion ($C = 14.18$ cm^3 K mol^{-1}). Upon cooling, the $\chi_m T$ value for the four complexes decreases gradually over the temperature range of 300–100 K and more rapidly below 100 K, which is mostly due to crystal-field effects (*i.e.* thermal depopulation of the Ln(III) ion Stark sublevels) and possible antiferromagnetic dipole–dipole interactions between the molecules.[23] Notably, the magnetic moment is still far from the theoretical value ($g_J \times J = 4/3 \times 15/2 = 10\ \mu_B$), which can reach 5.3 μ_B (**1**), 6.8 μ_B (**2**), 5.4 μ_B (**3**) and 5.1 μ_B (**4**) at 1.8 K. It is highly attributed to crystal field effects on the Dy(III) ion that eliminates the degeneracy of the $^6H_{15/2}$ ground state.[16a] The nonsuperimposition of the *M versus H*/*T* curves on a single curve reveals the existence of low-lying excited states and/or significant magnetic anisotropy in complexes **1–4** (Fig. 4, inset).[14d]

In addition, the field cooled (FC) and zero-field cooled (ZFC) magnetization measurements of complexes **1–4** were further performed (Fig. S16–S19 in the ESI†). These results unanimously suggest that the magnetization signals of complexes **1–4** are similar. The FC–ZFC curves show no divergence, certifying that there were no magnetic ordering and magnetic phase transition in accordance with $\chi_m T$ *vs.* *T* plots.

Dynamic magnetic properties

AC susceptibility curves of the complex **1** revealed the temperature dependent peaks in the in-of-phase (χ') and out-of-phase (χ'') *vs.* measurement (*T*) under the zero dc field, signaling "freezing" of the spins by the anisotropy barriers and indicating the presence of slow relaxation of the magnetization (Fig. 5).[10a] In addition, the low-frequency peaks occur in the lower temperature region. With increasing frequency, the maxima of the magnetic susceptibility shift to high temperature, which is the feature of a superparamagnet.[1b,17a,24] Only in the very low temperature region, below 2.5 K, there is a slight quantum tunneling effect, which can almost be ignored. Then a preliminary investigation into complexes **2–4** under the zero dc field was also conducted. However, the peaks can only be found at frequencies higher than 100 Hz for complexes **2** and **3**, and complex **4** shows only a poorly defined peak (Fig. S3–S5 in the ESI†). Upon cooling, χ'' increases again below 3.0 K for complexes **2** and **3**, and this indicates the onset of pure quantum, as often seen in other lanthanide SMMs.[10a] The applied dc field is required to suppress the QTM and is able to slow the temperature dependent maxima to the slowest relaxation frequency. Then, subsequent studies with an applied dc field of 2000 Oe revealed temperature dependent in-of-phase (χ') and out-of-phase (χ'') behavior. The complete ac experiment was conducted in a dc field of 2000 Oe, whereby the QTM has been effectively suppressed for complexes **1–4** (Fig. 6, and Fig. S6, and S7 in the ESI†).

A further investigation was conducted on complex **1** by a thorough in-of-phase (χ') and out-of-phase (χ'') *vs.* frequency (ν) measurement at temperatures between 2 and 12 K under the zero dc field (Fig. 7). A fit to the Arrhenius law $\tau = \tau_0 \exp(E_a/k_B T)$ of the peak maxima gave an energy barrier of $E_a = 56.7$ K and a pre-exponential time constant of $\tau_0 = 3.7 \times 10^{-7}$. Although this phenomenon was not observed under the zero dc field for complexes **2–3** (Fig. S8, S9 in the ESI†), it was found under a 2000 Oe field, with frequency dependence of in-phase (χ') and out-of-phase (χ'') ac susceptibility of $E_a = 28.7$ K, $\tau_0 = 2.5 \times 10^{-7}$ for complex **2** and $E_a = 27.8$ K, $\tau_0 = 1.0 \times 10^{-6}$ for complex **3**, respectively (Fig. 8). Unfortunately, this frequency dependence phenomenon was not observed for complex **4** under any dc field.

Obviously, the barrier height (U_{eff}/k_B) from complexes **1** to **3** takes on a depressive tendency, which is correlated to the

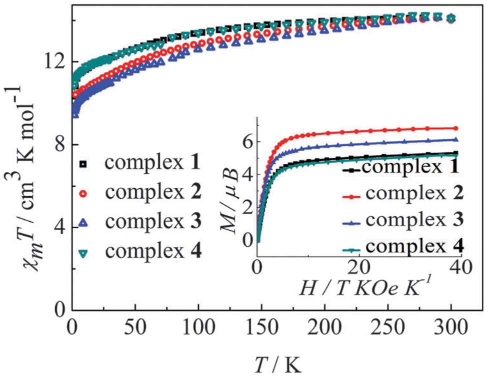

Fig. 4 Temperature dependence of $\chi_m T$ at 100 Oe for complexes **1–4** in the range 1.8–300 K. Inset: Field dependence of magnetization for complexes **1–4** at 1.8 K.

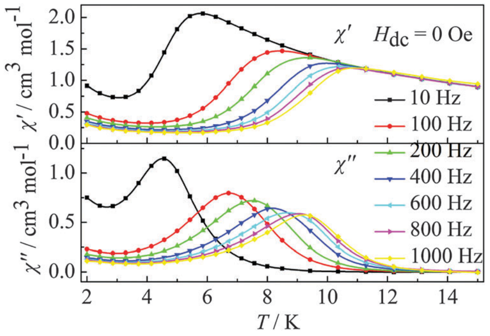

Fig. 5 Temperature dependence of the in-phase (χ') and out-of-phase (χ'') ac susceptibility of complex **1** under 0 Oe in the frequency range 10–1000 Hz.

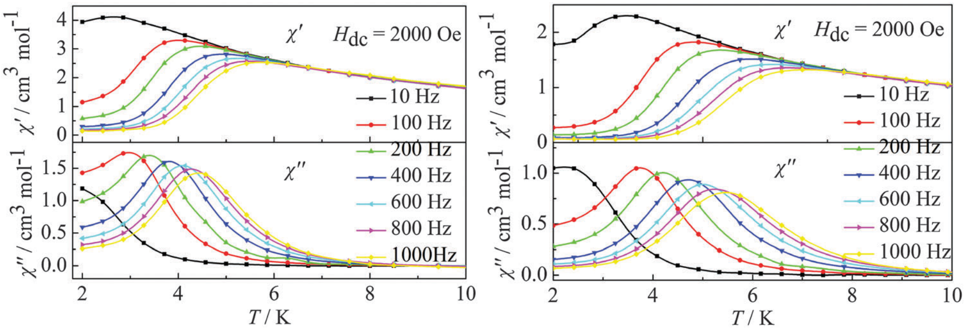

Fig. 6 Temperature dependence of the in-phase (χ') and out-of-phase (χ'') ac susceptibility of complexes **2** (left) and **3** (right) under 2000 Oe in the frequency range 10–1000 Hz.

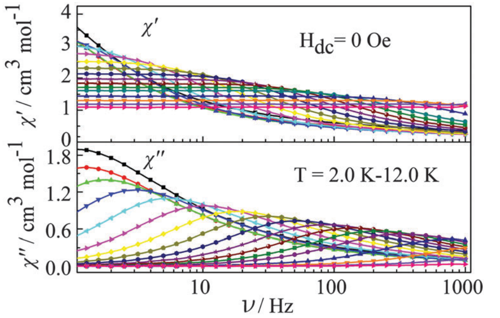

Fig. 7 Frequency dependence of the in-phase (χ') and out-of-phase (χ'') ac susceptibility under 0 Oe in the temperature range 2.0–12 K for complex **1**.

distortion of the coordination geometry around the center Dy(III) ion due to different auxiliary ligands. As we can see from the structural descriptions, complex **1**, first of all, is the most close to an ideal C_{3v}-capped octahedron with the high symmetry while complexes **2–4** are deviated more from the ideal C_{3v}-capped octahedron, which is in good agreement with the magnetic properties. On the other hand, due to the Kramer ion of the Dy(III) ion, the shortest distances of *l* and *d* in complex **1** enable the Dy(III) ion to be a more oblate electron, generating strong single-ion anisotropy for SMM.[25] Herein the distances of *l* and *d* in complexes **2–4** are all longer than complex **1**, leading to weaker single-ion anisotropy. On the basis of the above two aspects, the slight differences may affect the nature of single-ion anisotropy of the Dy(III) ion through the single-axial degree of distortion of coordination geometry, and therefore generates the different dynamic magnetic behavior for complexes **1–4**. In contrast with our previous report[17c] and another groups' report,[11b,16a,b,26] the energy barrier for complex **1** is higher than those of mononuclear lanthanide complexes based on common β-diketone ligands, suggesting the larger local symmetry and the ligand field effect in our present system. However, the energy barrier for complex **1** is still lower than that observed for a series of classical eight-coordinated mononuclear [Dy(acac)-auxiliary] complexes.[10b,17a,b] The main reason is attributed to the decreased coordination numbers and molecular symmetry, as well as the weakened strength of the ligand field.[21a] According to the ac susceptibility of frequency and the temperature dependence between 2.0 and 12.0 K, the magnetization relaxation time τ of complex **1** is 0.0997 s (Fig. 9). Notably, the relaxation time of complex **1** is the longest among those previously reported for the pure β-diketone dysprosium analogue with D_{4d} and D_{2d} symmetry,[10a,b,17] further proving that, above 2.5 K, the relaxation becomes thermally activated (Arrhenius-like behavior), unlike the traditional eight-coordinated geometry β-diketone dysprosium complexes with coexisting thermally activated and quantum tunneling regimes. This system has almost no obvious quantum regime in the whole temperature range.

Cole–Cole plots of the ac data of complex **1** can be fitted to the generalized Debye model (Fig. 10), where χ_T is the isothermal

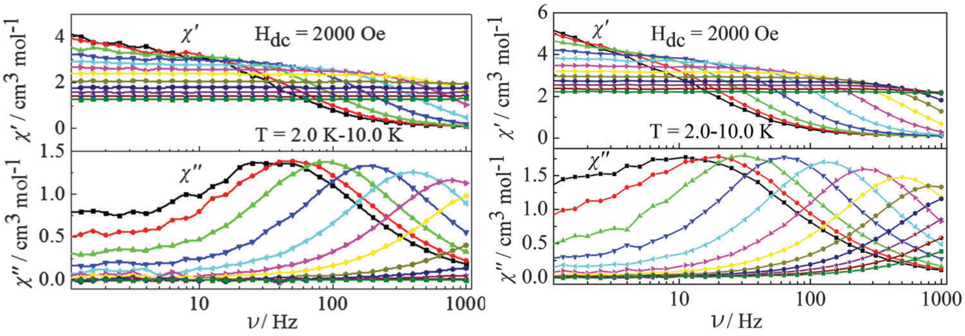

Fig. 8 Frequency dependence of the in-phase (χ') and out-of-phase (χ'') ac susceptibility under 2000 Oe in the temperature range 2.0–10 K for complexes **2** (left) and **3** (right).

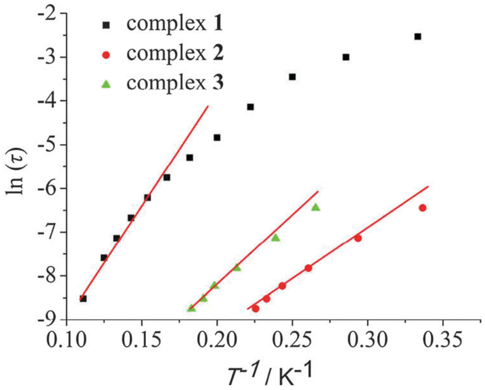

Fig. 9 Arrhenius plot showing the relaxation time of the magnetization for complex **1** under 0 Oe, complexes **2** and **3** under 2000 Oe. Red line is a fit to the Arrhenius equation.

susceptibility, χ_S is the adiabatic susceptibility, ν is the frequency of the ac field, and τ is the relaxation time of the system.[20,21,27]

$$\chi_{(\nu)} = \chi_S + \frac{\chi_T - \chi_S}{1 + (i\nu\tau)^{1-\alpha}}$$

However, on the basis of the Cole–Cole analysis, τ_0 is still larger than expected for a thermally activated relaxation mechanism for complex **1** under 0 Oe. This may be partially explained by large *a* values for the modified Debye fit of complex **1**, where between 10 and 2 K α values are 0.09–0.30 and they increase significantly at lower temperatures (Table 4). The result indicates that a single relaxation time is mainly involved in the present relaxation process. The Cole–Cole plots for complexes **2** and **3** give the same semicircle plots under 2000 Oe (Fig. S10 in the ESI†), where between 5 and 2 K α values are 0.09–0.21 for complex **2** and 0.09–0.28 for complex **3** (Table S2, ESI†). It is worth noting that Cole–Cole plots of complex **1** are familiar with the 1: 20 dilution sample of the Gao and Tang group,[10a] proving the weak dipole–dipole interactions between the dysprosium centers. Weakened dipole–dipole interactions further illustrate complex **1** as being the most close to the ideal C_{3v}-capped octahedron with almost no QTM. However, complexes **2–4** deviated more from an ideal C_{3v}-capped octahedron indicating a more QTM effect.

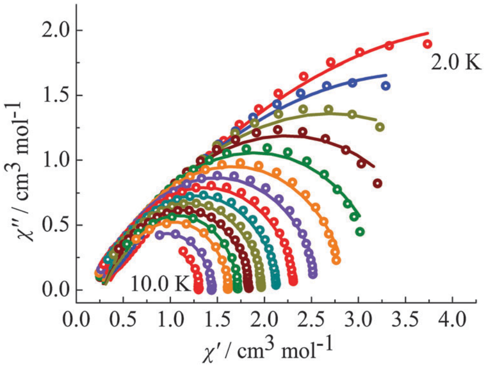

Fig. 10 Cole–Cole plots measured at 2.0–10.0 K under 0 Oe for complex **1**.

Table 4 Fitted parameters of the Cole–Cole plots for complex **1** at H_{dc} = 0 Oe

T/K	χ_S	χ_T	α	T/K	χ_S	χ_T	α
2.0	0.43244	5.52038	0.25926	6.0	0.28812	2.15754	0.15739
2.5	0.35860	4.82926	0.26597	6.5	0.31634	1.98911	0.13895
3.0	0.28189	4.75016	0.30403	7.0	0.34146	1.84919	0.12536
3.5	0.25763	3.93669	0.26994	7.5	0.39825	1.72553	0.09065
4.0	0.25813	3.32001	0.23068	8.0	0.40657	1.62146	0.09204
4.5	0.25387	2.90182	0.20615	9.0	0.43839	1.44561	0.09024
5.0	0.24698	2.60083	0.19324	10.0	0.53813	1.30842	0.09236
5.5	0.26152	2.35780	0.17661				

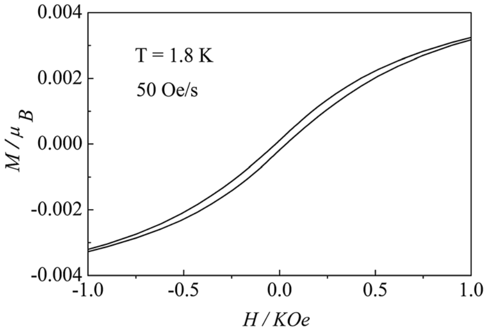

Fig. 11 Hysteresis loop for complex **1** at 1.8 K.

Magnetic hysteresis is another important characteristic of the magnetic bistability of SMMs. When the dc magnetism is conducted at 1.8 K with a sweep rate of 50 Oe s^{-1}, the hysteresis loops of complex **1** are wider than those for complexes **2** and **3** within ±4 kOe (Fig. 11, Fig. S11 in the ESI†). The M–H data do not exhibit a hysteresis phenomenon at 1.8 K for complex **4**. This further suggests that complexes **1–3** are typical SMMs.

Conclusion

Isolation of a series of four EIFD dysprosium lanthanide complexes **1–4** verifies that the newly designed β-diketone EIFD is able to stabilize the Dy(III) ion forming unique seven-coordinated mononuclear Dy(III) complexes with C_{3v} symmetry which afford the SMMs of complexes **1–4**. The introduction of the auxiliary ligands of DMF, DMSO and TPPO slightly tunes the distortion of the coordination symmetry and the ligand field around the Dy(III) ion. It results in the difference of the energy barriers between complexes **1–4**. Namely, the higher symmetry of the coordination geometry results in the higher energy barriers. Notably, QTM is more effectively suppressed in this system, which is more related to the less deviation from the ideal C_{3v} symmetry. Therefore, this approach may provide an effective path to suppress the QTM, which universally exists in the lanthanide complexes.

Notes

The authors declare no competing financial interest.

Acknowledgements

This work is financially supported by the National Natural Science Foundation of China (No. 21471051, 51272069 and 51402092).

References

1 (*a*) P. Zhang, L. Zhang, C. Wang, S. Xue, S. Y. Lin and J. Tang, *J. Am. Chem. Soc.*, 2014, **136**, 4484–4487; (*b*) J. J. Le Roy, M. Jeletic, S. I. Gorelsky, I. Korobkov, L. Ungur, L. F. Chibotaru and M. Murugesu, *J. Am. Chem. Soc.*, 2013, **135**, 3502–3510.

2 (*a*) N. Ishikawa, M. Sugita, T. Ishikawa, S.-y. Koshihara and Y. Kaizu, *J. Am. Chem. Soc.*, 2003, **125**, 8694–8695; (*b*) N. Magnani, C. Apostolidis, A. Morgenstern, E. Colineau, J. C. Griveau, H. Bolvin, O. Walter and R. Caciuffo, *Angew. Chem., Int. Ed.*, 2011, **50**, 1696–1698; (*c*) S. D. Jiang, B. W. Wang, H. L. Sun, Z. M. Wang and S. Gao, *J. Am. Chem. Soc.*, 2011, **133**, 4730–4733; (*d*) D. P. Li, T. W. Wang, C. H. Li, D. S. Liu, Y. Z. Li and X. Z. You, *Chem. Commun.*, 2010, **46**, 2929–2931; (*e*) M. A. AlDamen, J. M. Clemente-Juan, E. Coronado, C. Martí-Gastaldo and A. Gaita-Ariño, *J. Am. Chem. Soc.*, 2008, **130**, 8874–8875.

3 R. Sessoli, H. L. Tsai, A. R. Schake, S. Wang, J. B. Vincent, K. Folting, D. Gatteschi, G. Christou and D. N. Hendrickson, *J. Am. Chem. Soc.*, 1993, **115**, 1804–1816.

4 A. Caneschi, D. Gatteschi, R. Sessoli, A. L. Barra, L. C. Brunel and M. Guillot, *J. Am. Chem. Soc.*, 1991, **113**, 5873–5874.

5 D. N. Woodruff, R. E. Winpenny and R. A. Layfield, *Chem. Rev.*, 2013, **113**, 5110–5148.

6 (*a*) R. Sessoli and A. K. Powell, *Coord. Chem. Rev.*, 2009, **253**, 2328–2341; (*b*) F. Habib and M. Murugesu, *Chem. Soc. Rev.*, 2013, **42**, 3278–3288; (*c*) L. Sorace, C. Benelli and D. Gatteschi, *Chem. Soc. Rev.*, 2011, **40**, 3092–3104.

7 N. F. Chilton, S. K. Langley, B. Moubaraki, A. Soncini, S. R. Batten and K. S. Murray, *Chem. Sci.*, 2013, **4**, 1719–1730.

8 (*a*) L. Zhao, J. Wu, H. Ke and J. Tang, *CrystEngComm*, 2013, **15**, 5301–5306; (*b*) S. Y. Lin, L. Zhao, Y. N. Guo, P. Zhang, Y. Guo and J. Tang, *Inorg. Chem.*, 2012, **51**, 10522–10528; (*c*) A. K. Jami, V. Baskar and E. C. Sanudo, *Inorg. Chem.*, 2013, **52**, 2432–2438; (*d*) B. Hussain, D. Savard, T. J. Burchell, W. Wernsdorfer and M. Murugesu, *Chem. Commun.*, 2009, 1100–1102; (*e*) D. T. Thielemann, M. Klinger, T. J. Wolf, Y. Lan, W. Wernsdorfer, M. Busse, P. W. Roesky, A. N. Unterreiner, A. K. Powell, P. C. Junk and G. B. Deacon, *Inorg. Chem.*, 2011, **50**, 11990–12000; (*f*) P. Hu, X. Wang, Y. Ma, Q. Wang, L. Li and D. Liao, *Dalton Trans.*, 2014, **43**, 2234–2243; (*g*) F. Habib, P.-H. Lin, J. Long, I. Korobkov, W. Wernsdorfer and M. Murugesu, *J. Am. Chem. Soc.*, 2011, **133**, 8830–8833; (*h*) J. Tang, I. Hewitt, N. T. Madhu, G. Chastanet, W. Wernsdorfer, C. E. Anson, C. Benelli, R. Sessoli and A. K. Powell, *Angew. Chem., Int. Ed.*, 2006, **45**, 1729–1733; (*i*) I. J. Hewitt, Y. Lan, C. E. Anson, J. Luzon, R. Sessoli and A. K. Powell, *Chem. Commun.*, 2009, 6765–6767.

9 F. Habib, G. Brunet, V. Vieru, I. Korobkov, L. F. Chibotaru and M. Murugesu, *J. Am. Chem. Soc.*, 2013, **135**, 13242–13245.

10 (*a*) Y. Bi, Y. N. Guo, L. Zhao, Y. Guo, S. Y. Lin, S. D. Jiang, J. Tang, B. W. Wang and S. Gao, *Chem. – Eur. J.*, 2011, **17**, 12476–12481; (*b*) G. J. Chen, Y. N. Guo, J. L. Tian, J. Tang, W. Gu, X. Liu, S. P. Yan, P. Cheng and D. Z. Liao, *Chem. – Eur. J.*, 2012, **18**, 2484–2487.

11 (*a*) S. Takamatsu, T. Ishikawa, S.-y. Koshihara and N. Ishikawa, *Inorg. Chem.*, 2007, **46**, 7250–7252; (*b*) Y. Wang, X. L. Li, T. W. Wang, Y. Song and X. Z. You, *Inorg. Chem.*, 2010, **49**, 969–976.

12 (*a*) N. Ishikawa, *J. Phys. Chem. A*, 2003, **107**, 5831–5835; (*b*) N. Ishikawa, M. Sugita, T. Ishikawa, S.-y. Koshihara and Y. Kaizu, *J. Phys. Chem. B*, 2004, **108**, 11265–11271; (*c*) N. Ishikawa, M. Sugita and W. Wernsdorfer, *Angew. Chem., Int. Ed.*, 2005, **44**, 2931–2935; (*d*) W. H. Harman, T. D. Harris, D. E. Freedman, H. Fong, A. Chang, J. D. Rinehart, A. Ozarowski, M. T. Sougrati, F. Grandjean, G. J. Long, J. R. Long and C. J. Chang, *J. Am. Chem. Soc.*, 2010, **132**, 18115–18126.

13 D. P. Li, X. P. Zhang, T. W. Wang, B. B. Ma, C. H. Li, Y. Z. Li and X. Z. You, *Chem. Commun.*, 2011, **47**, 6867–6869.

14 (*a*) P. P. Lima, M. M. Nolasco, F. A. A. Paz, R. A. S. Ferreira, R. L. Longo, O. L. Malta and L. D. Carlos, *Chem. Mater.*, 2013, **25**, 586–598; (*b*) J. Shi, Y. Hou, W. Chu, X. Shi, H. Gu, B. Wang and Z. Sun, *Inorg. Chem.*, 2013, **52**, 5013–5022; (*c*) J. Li, H. Li, P. Yan, P. Chen, G. Hou and G. Li, *Inorg. Chem.*, 2012, **51**, 5050–5057; (*d*) G. Abbas, Y. Lan, G. E. Kostakis, W. Wernsdorfer, C. E. Anson and A. K. Powell, *Inorg. Chem.*, 2010, **49**, 8067–8072; (*e*) S. Biju, Y. K. Eom, J.-C. G. Bünzli and H. K. Kim, *J. Mater. Chem. C*, 2013, **1**, 6935–6944; (*f*) M. Pietraszkiewicz, M. Maciejczyk, I. D. W. Samuel and S. Zhang, *J. Mater. Chem. C*, 2013, **1**, 8028–8032; (*g*) V. Divya and M. L. P. Reddy, *J. Mater. Chem. C*, 2013, **1**, 160–170.

15 K. Bernot, J. Luzon, L. Bogani, M. Etienne, C. Sangregorio, M. Shanmugam, A. Caneschi, R. Sessoli and D. Gatteschi, *J. Am. Chem. Soc.*, 2009, **131**, 5573–5579.

16 (*a*) Y. L. Wang, Y. Ma, X. Yang, J. Tang, P. Cheng, Q. L. Wang, L. C. Li and D. Z. Liao, *Inorg. Chem.*, 2013, **52**, 7380–7386; (*b*) C. M. Liu, D. Q. Zhang and D. B. Zhu, *Inorg. Chem.*, 2013, **52**, 8933–8940; (*c*) W. B. Sun, B. L. Han, P. H. Lin, H. F. Li, P. Chen, Y. M. Tian, M. Murugesu and P. F. Yan, *Dalton Trans.*, 2013, **42**, 13397–13403.

17 (*a*) S. D. Jiang, B. W. Wang, G. Su, Z. M. Wang and S. Gao, *Angew. Chem., Int. Ed.*, 2010, **49**, 7448–7451; (*b*) G. J. Chen, C. Y. Gao, J. L. Tian, J. K. Tang, W. Gu, X. Liu, S. P. Yan, D. Z. Liao and P. Cheng, *Dalton Trans.*, 2011, **40**, 5579–5583; (*c*) J. Zhu, C. Z. Wang, F. Luan, T. Q. Liu, P. F. Yan and G. M. Li, *Inorg. Chem.*, 2014, **53**, 8895–8901.

18 G. M. Sheldrick, *ActaFound. Crystallogr.*, 2008, **64**, 112–122.

19 A. Bellusci, G. Barberio, A. Crispini, M. Ghedini, M. La Deda and D. Pucci, *Inorg. Chem.*, 2005, **44**, 1818–1825.

20 E. L. Muetterties and L. J. Guggenberger, *J. Am. Chem. Soc.*, 1974, **96**, 1748–1756.

21 (*a*) F. Gao, L. Cui, W. Liu, L. Hu, Y. W. Zhong, Y. Z. Li and J. L. Zuo, *Inorg. Chem.*, 2013, **52**, 11164–11172; (*b*) M. X. Yao, Q. Zheng, F. Gao, Y. Z. Li, Y. Song and J. L. Zuo, *Dalton Trans.*, 2012, **41**, 13682–13690.

22 (*a*) M. L. Kahn, R. Ballou, P. Porcher, O. Kahn and J.-P. Sutter, *Chem. – Eur. J.*, 2002, **8**, 525–531; (*b*) M. L. Kahn, J.-P. Sutter, S. Golhen, P. Guionneau, L. Ouahab, O. Kahn and D. Chasseau, *J. Am. Chem. Soc.*, 2000, **122**, 3413–3421.

23 G. Abbas, Y. Lan, G. E. Kostakis, W. Wernsdorfer, C. E. Anson and A. K. Powell, *Inorg. Chem.*, 2010, **49**, 8067–8072.

24 Y. Ma, G. F. Xu, X. Yang, L. C. Li, J. Tang, S. P. Yan, P. Cheng and D. Z. Liao, *Chem. Commun.*, 2010, **46**, 8264–8266.

25 J. D. Rinehart and J. R. Long, *Chem. Sci.*, 2011, **2**, 2078–2085.

26 (*a*) P. Hu, M. Zhu, X. Mei, H. Tian, Y. Ma, L. Li and D. Liao, *Dalton Trans.*, 2012, **41**, 14651–14656; (*b*) G. J. Chen, Y. Zhou, G. X. Jin and Y. B. Dong, *Dalton Trans.*, 2014, **43**, 16659–16665; (*c*) Y.-L. Wang, B. Gu, Y. Ma, C. Xing, Q.-L. Wang, L.-C. Li, P. Cheng and D.-Z. Liao, *CrystEngComm*, 2014, **16**, 2283–2289; (*d*) M. Menelaou, F. Ouharrou, L. Rodriguez, O. Roubeau, S. J. Teat and N. Aliaga-Alcalde, *Chem. – Eur. J.*, 2012, **18**, 11545–11549; (*e*) D. Zeng, M. Ren, S. S. Bao and L. M. Zheng, *Inorg. Chem.*, 2014, **53**, 795–801; (*f*) L. Norel, M. Feng, K. Bernot, T. Roisnel, T. Guizouarn, K. Costuas and S. Rigaut, *Inorg. Chem.*, 2014, **53**, 2361–2363.

27 S. M. J. Aubin, Z. Sun, L. Pardi, J. Krzystek, K. Folting, L.-C. Brunel, A. L. Rheingold, G. Christou and D. N. Hendrickson, *Inorg. Chem.*, 1999, **38**, 5329–5340.